doi:10.1016/j.jmb.2006.11.040 J. Mol. Biol. (2007) 366, 602–610

JMB

Available online at www.sciencedirect.com

ScienceDirect

ELSEVIER

Intermolecular Interactions and Characterization of the Novel Factor Xa Exosite Involved in Macromolecular Recognition and Inhibition: Crystal Structure of Human Gla-domainless Factor Xa Complexed with the Anticoagulant Protein NAPc2 from the Hematophagous Nematode *Ancylostoma caninum*

M. T. Murakami[1], J. Rios-Steiner[2], S. E. Weaver[2], A. Tulinsky[2] J. H. Geiger[2]* and R. K. Arni[1,3]*

[1]*Department of Physics IBILCE/UNESP, São José do Rio Preto, SP 15054-000, Brazil*

[2]*Department of Chemistry Michigan State University East Lansing, MI 48824-1322 USA*

[3]*Center for Applied Toxinology CAT-CEPID, São Paulo SP 05503-900, Brazil*

**Corresponding authors*

NAPc2, an anticoagulant protein from the hematophagous nematode *Ancylostoma caninum* evaluated in phase-II/IIa clinical trials, inhibits the extrinsic blood coagulation pathway by a two step mechanism, initially interacting with the hitherto uncharacterized factor Xa exosite involved in macromolecular recognition and subsequently inhibiting factor VIIa (K_i=8.4 pM) of the factor VIIa/tissue factor complex. NAPc2 is highly flexible, becoming partially ordered and undergoing significant structural changes in the C terminus upon binding to the factor Xa exosite. In the crystal structure of the ternary factor Xa/NAPc2/selectide complex, the binding interface consists of an intermolecular antiparallel β-sheet formed by the segment of the polypeptide chain consisting of residues 74–80 of NAPc2 with the residues 86–93 of factor Xa that is additional maintained by contacts between the short helical segment (residues 67–73) and a turn (residues 26–29) of NAPc2 with the short C-terminal helix of factor Xa (residues 233–243). This exosite is physiologically highly relevant for the recognition and inhibition of factor X/Xa by macromolecular substrates and provides a structural motif for the development of a new class of inhibitors for the treatment of deep vein thrombosis and angioplasty.

Keywords: factor Xa exosite; nematode anticoagulant protein; selectide inhibitor; factor VIIa/tissue factor complex; inhibition

Introduction

Vascular injuries prompt the activation of an intricate and balanced cascade of reactions that involve a number of serine proteases and macromolecular cofactors ultimately culminating in the formation of a stable, cross-linked clot to stem blood loss. Factor Xa (fXa) plays a pivotal and central role in the coagulation cascade by uniting the intrinsic and extrinsic pathways and also by participating in the formation of the prothrombinase complex (prothrombin/fXa/factor Va/cellular surface/Ca^{+2}) that converts prothrombin to thrombin by limited proteolysis.[1] Thrombin subsequently reacts with fibrinogen to produce the fibrin network. The factor

Present address: J. Rios-Steiner, Department of Chemistry, University of Puerto Rico, Mayaguez, Puerto Rico.

Abbreviations used: fXa, activated factor X; Gla, γ-carboxyglutamic acid; EGF, epidermal growth factor; NAPs, nematode anticoagulant proteins; fVIIa, activated factor VII; TAP, tick anticoagulant protein; TF, tissue factor; des-fXa, fXa less its γ-carboxyglumatic domain; r.m.s.d., root mean square deviations.

E-mail addresses of the corresponding authors: geiger@cem.msu.edu; arni@ibilce.unesp.br

X (fX) light chain consists of an N-terminal Gla domain (post-translationally modified γ-carboxy-glutamate residues)[2] and two epidermal-growth-factor-like (EGF) domains.[3,4] The heavy chain, which harbors the serine protease catalytic domain, shares extensive structural and sequential homology with other vitamin K-dependent serine proteases.[5]

Thrombosis, abnormal blood coagulation, occurs in a variety of cardiac disorders including angina, pulmonary embolism, atrial fibrillation, post myocardial infarction, and stroke. Nematode anticoagulant proteins (NAPs) from the hematophagous nematode *Ancylostoma caninum* inhibit blood coagulation and have been targeted as potential therapeutic agents for the control and regulation of thrombosis.[6,7] The NAPs, specifically NAP5, NAP6 and NAPc2, are small (75–84 amino acid residues) disulfide linked proteins that preferentially inhibit fXa and factor VIIa (fVIIa). NAP5 inhibits the amidolytic activity of fXa with a $K_i = 43$ pM; the only other natural inhibitor of fXa comparable to NAP5 is tick anticoagulant peptide (TAP) ($K_i = 59$ pM).[8] NAP6, a highly homologous member of the family, inhibits the catalytic activity of fXa with a K_i ~1.0 nM. TAP, NAP5 and NAP6, inhibit thrombin formation by direct association at the catalytic site of fXa. NAPc2 only partially inhibits the amidolytic activity of fXa and prevents the formation of α-thrombin by binding to a site distinct and remote from the active site, thus representing the basis for the development of a promising new class of fXa exosite inhibitors. The resultant binary complex inactivates the tissue factor (TF)-fVIIa complex with a $K_i = 8.4$ pM.[7] Isothermal titration calorimetry and fluorescence experiments indicate that the COOH terminus of the heavy chain of human fXa contributes to the high affinity interaction with NAPc2 however; the structural details of this interaction have not been characterized.[9] NMR results of NAPc2 indicate that the core is principally stabilized by five-disulfide bridges and two β sheets, each composed of two short antiparallel strands and that the molecule is highly flexible, exhibiting large amplitude structural variations at both the N and C termini and in the reactive-site binding loop.

Current clinical strategies for the control of blood coagulation are primarily based on molecules derived from coumarins that inhibit the post-translational γ-carboxylation of glutamate residues on vitamin K-dependent coagulations factors and heparin analogues that enhance inhibition of thrombin and fXa by antithrombin III. These anticoagulants are non-selective and display therapeutic limitations in their ability to maintain the balance of the haemostatic system, thus providing the impetus for the search and development of new exosite anticoagulants with high macromolecular selectivity and low harmful side effects. NAPc2 represents a new class of the TF/fVIIa pathway inhibitors that is significantly more potent and specific than low molecular weight heparins and it is undergoing clinical trials to evaluate their utility as anticoagulants. NAPc2 is in Phase II clinical trials for the treatment and prevention of deep vein thrombosis following orthopedic surgery and in Phase IIa trials in angioplasty patients.

The crystal structure of human Gla-domainless fXa (des-fXa) complexed with recombinant NAPc2 determined at 2.2 Å resolution demonstrates that NAPc2 binds in a shallow surface depression at the COOH terminus of fXa that is parallel to the β-strand (β5) of the barrel, extending to the 60s-loop. This novel exosite on fXa could serve as a platform for the design of new drugs for the treatment of haemostatic disorders.

Results and Discussion

Overall structure of the ternary complex

Crystallographic refinement of the ternary complex fXa-NAPc2-selectide at 2.2 Å resolution converged to a crystallographic residual of 22.1% ($R_{free} = 26.7\%$). The asymmetric unit contains one des-fXa molecule (catalytic and EGF2 domains), one NAPc2 molecule, a selectide inhibitor (TyrD-Ile-Arg-Leu-PrN), one Na^+, three acetate and six PO_4^{2-} ions. Analysis of the stereochemistry of the final model indicates that the main-chain dihedral angles for all residues are located in the permitted regions of the Ramachandran diagram and that the root mean square deviations (r.m.s.d.) from ideal values are distributed within the expected ranges for well-refined structures (Table 1). Except for a few side-chains, which are present on the surface, the C-terminal EGF2 domain and the catalytic domain of des-fXa are well defined in the final ($2F_o–F_c$) electron density map. The entire N-terminal EGF1 domain, and its leading pentapeptide, which is flexibly disordered in other des-fXa structures[10–12] was not located in the electron density maps. As observed in other inhibited fXa structures,[11–13] there are no apparent cleavages in the autolysis loop region of the ternary complex (His145–Thr153) as reported for the native structure.[10] Optimal superpositioning of the C^α positions of the catalytic and EGF2 domains of the ternary complex on those of the native fXa (PDB code 1HCG) results in a r.m.s.d. of 0.46 Å for 256 of a total of 292 C^α atoms; a shift is observed in the 72–80 loop and additional deviations are principally located in the autolysis loop region.

The sodium-binding site first characterized in fXa[14] was subsequently identified in thrombin[15] and activated protein C.[16] In the structures of fXa and thrombin, the Na^+ is sandwiched between the 184–189 and 221–225 loops.[17] Similarly, the Na+ in the ternary complex structure is penta-coordinated by the carbonyl oxygen atoms of Tyr184 (3.05 Å), Lys186 (3.22 Å), Arg222 (2.94 Å), Lys224 (3.09 Å) and a water molecule, 43W (2.89 Å). Interestingly, each of the opposite faces of the 184–189 and 221–225 loops are coordinated by a PO_4^{2-} (Figure 1(a)). In the 184–189 loop, the PO_4^{2-} is coordinated by main-

Table 1. Data collection and refinement statistics

Crystal preparation	
Cryoprotectant solution	20% glycerol
Soaking time	20 s
Data collection	
Wavelength (Å)	1.00
Temperature (K)	100
Detector	MARCCD
Synchrotron radiation source	Advanced Photon Source-IMCA-CAT beamline
Space group	$P2_12_12_1$
Unit cell parameters (Å)	$a=48.95$, $b=86.41$, $c=145.89$
Resolution (Å)	40.0–2.2
N° molecules in the asymmetric unit	1 fXa+ 1 NAPc2+ 1 selectide
Solvent content (%)	66.9
V_M ($Å^3Da^{-1}$)	3.7
N° reflections	498,336
N° unique reflections	32,280 (2.27)
$I/\sigma<I>$	21.5 (7.5)
Multiplicity	7.5 (7.0)
Completeness (%)	100.0 (99.7)
R_{merge} [a] (%)	6.8 (22.2)
Structure refinement statistics	
R_{factor} (%)	21.9
R_{free} (%)	26.9
r.m.s.d. bond distances (Å)	0.024
r.m.s.d. bond angles (°)	2.14
Average *B*-factors ($Å^2$)	45.4
Ramachandran plot Analysis	
Residues in most favored regions (%)	81.4
Residues in allowed regions (%)	14.7
Residues in generously allowed regions (%)	3.9
Residues in disallowed regions (%)	0
Number of non-glycine residues	285
Final model	
Number of amino acid residues	326
Number of modeled water molecules	260
Number of phosphate ions	6
Number of acetate ions	3
Number of sodium ions	1

Statistical values for the highest resolution shells are given in parentheses.

[a] $R_{merge}=\Sigma|I(h)_I-\{I(h)\}|/\Sigma\{I(h)\}$, where I_h is the observed intensity of the *i*th measurement of reflection *h* and $\{I(h)\}$ is the mean intensity of reflection *h* calculated after scaling.

chain amide N–H groups of residues Asp185A (phosphate O1 atom, 2.69 Å), Thr185B (phosphate O3 atom, 2.53 Å), Lys186 (phosphate O2 atom, 2.94 Å) and a water molecule 57W (phosphate O4 atom, 3.22 Å) (Figure 1(a)). In the 221–225 loop, the PO_4^{2-} occludes the entrance to the sodium-binding site by interacting with Glu187NE2 (phosphate O3 atom, 3.12 Å), Lys223 (phosphate O3 atom, 2.47 Å) and solvent molecules 146W and 415W (phosphate O4 atom, 2.89 and 2.63 Å, respectively). As in fVIIa,[18] factor IXa[19] and trypsin,[20] fXa also possesses a calcium-binding site in the catalytic domain formed by the 70–80 loop, however, no electron density that could be attributed to the presence of the Ca^{2+} was observed in this region.

Interactions between fXa and the selectide inhibitor

The selectide inhibitor represents a new class of fXa inhibitors and is formed by a penta-peptide containing a N-terminal D-tyrosine, followed by isoleucine, arginine, leucine and terminates with a modified proline possessing a carboxamide group instead of a carboxyl group. The selectide inhibitor binds in the active-site cleft occupying the S1, S2 and acyl binding sites. Despite the high specificity of fXa for arginine residues in the S1 specificity pocket, TyrD1 occupies this sub-site and the hydroxyl group of TyrD1 interacts *via* a water molecule with the carbonyl oxygen of Ile227 and the side-chain carboxylate oxygen of Asp189OD1 (Figure 1(b)). Additionally, TyrD1N is hydrogen bonded to the

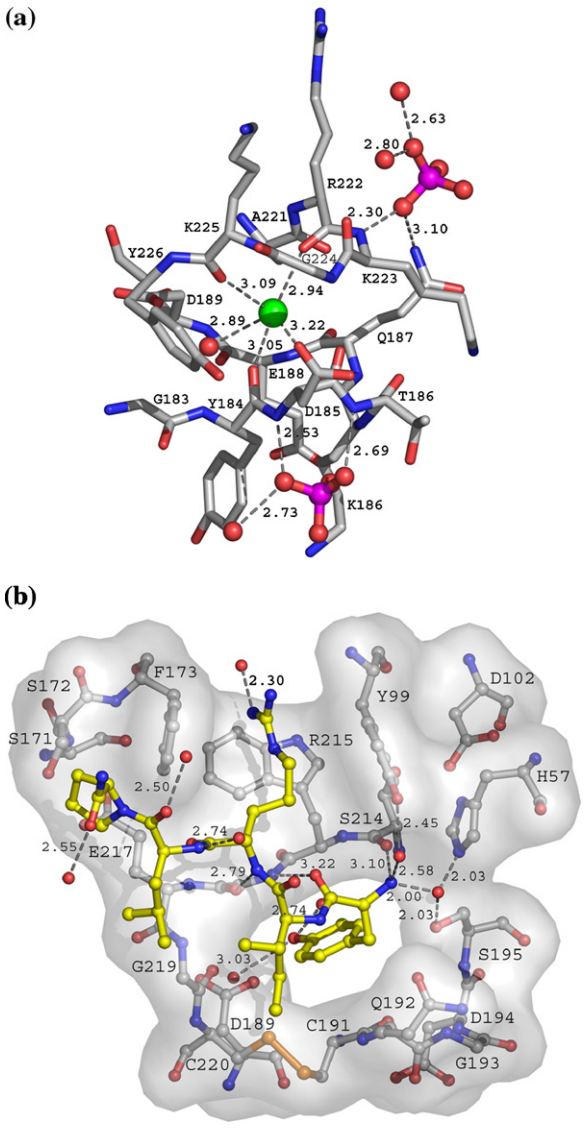

Figure 1. Interactions formed in: (a) the sodium-binding site (carbon in gray; sodium in green; phosphate in pink and red); and (b) the active-site pocket of fXa (carbon in gray) by the selectide inhibitor (carbon in yellow).

carbonyl oxygen of Ser214 and interacts with His57NE2 and Ser195OH *via* a water molecule (Figure 1(b)). Arg3NH2 of the selectide inhibitor also participates in a water-mediated interaction with the carbonyl oxygen of Ile174. The plane of the positively charged guanidinium group of Arg3 stacks parallel to the π-electron face of Phe174 of fXa (contacts <3.5 Å) leading to a cation-π electron-mediated interaction or ion-quadrupole attraction,[21–24] which appears to be unique to fXa (Figure 1(b)).[11,12,25,26] The phenyl group of Phe174 is slightly displaced by the encroaching guanidinium group of Arg3 of selectide compared to native fXa. Two other aromatic residues in the vicinity (Tyr99, Trp215) have also been implicated to play a role in the cation recognition interaction by fXa.[11,24,26] Additional contacts that occur between fXa and the selectide inhibitor are presented in Table 2.

Binding and conformational changes of NAPc2

NMR results indicate that NAPc2 is extremely flexible and it has been suggested that it is likely to become structured upon binding to fXa.[27] The β-strands and the two turns of α-helix are fairly well-defined in all 18 different NMR structures of NAPc2. Our crystallographic results indicate that NAPc2 only becomes partially structured after binding to fXa. Based on the electron density maps, we were able to construct the 6–13 and 21–30 regions and the C-terminal extension (50–83 residues) of NAPc2 (Figure 2(a) and (b)). The rest of the molecule is highly disordered and the electron density maps are characterized by diffuse electron density. The first residue observed is Cys6 that forms a disulfide bridge with Cys50. The next disordered region encompasses Cys14 to Glu20. Cys15 forms a disulfide bridge with Cys46; Cys46 is also part of a large, disordered region of NAPc2, which encompasses residues Glu31 to Asp49. The C-terminal region is mostly ordered and a dramatic conformational change occurs at the C terminus of NAPc2 when bound to fXa compared to the relative orientation of the C terminus observed in the NMR structure of NAPc2 (Figure 2(a)). The binding interface consists of an intermolecular antiparallel β-sheet formed between the segments comprised of residues 86–93 of fXa (residue numbering based on chymotrypsinogen)[28] and the C terminus (residues 74–80) of NAPc2 (Figure 3(c)) and additionally involves interactions between the 61–65 segment of fXa and the C-terminal extension (residues 81–83) of NAPc2. Other important contacts forming hydrogen bonds involve the 26–29 turn and the 67–73 helix from NAPc2 with the short C-terminal helix of fXa (a complete list of contacts is presented in Table 2). The interactions formed between NAPc2 and fXa are principally restricted to the well-ordered regions

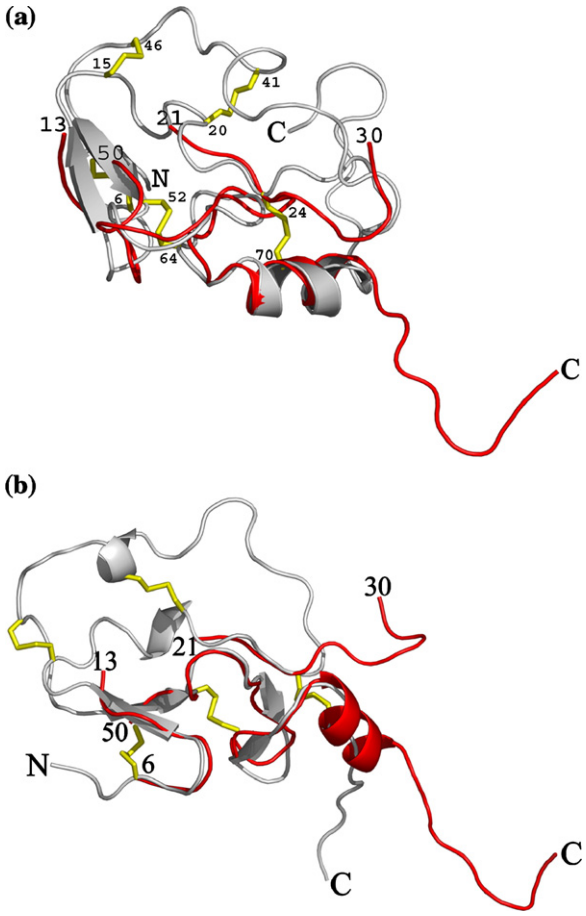

Figure 2. Overlays of the NAPc2 crystallographic structure (red) on (a) the NMR-derived average structure (gray); and (b) crystallographic structure of NAP5 (gray; J.R.S. and A.T., unpublished results).

Table 2. Hydrogen bond interactions formed between NAPc2 and fXa, and selectide and fXa

NAPc2	fXa	Distance (Å)
Asp27OD1	Arg125NH2	2.38
Asp27OD2	Trp237N	3.02
Asp27OD2	Leu235N	3.28
Asp27OD2	Lys236N	2.94
Asp27OD2	Arg125NH2	2.96
Gly28O	Asn178ND2	2.86
Glu68OE2	Lys243NZ	2.79
Asp69OD2	Arg240NH1	3.07
Asp73O	Asn9ND2	2.99
Asn74OD1	Arg93NE	3.35
Asn74O	Asn92N	2.86
Asn74O	Trp237NE1	3.18
Asp76N	Lys90O	3.31
Asp76O	Lys90N	2.90
Ile78N	Val88O	3.25
Ile78O	Val88N	2.66
Gly81O	Lys62O	2.65
Thr82N	Lys62O	2.52
Arg83N	Ala61O	2.97
Arg83N	Tyr60O	2.54
Selectide	**fXa**	**Distance (Å)**
TyrD1N	Ser214O	3.10
TyrD1N	His57NE2	3.16
TyrD1O	Gly216N	3.24
Arg3N	Gly216O	2.79
Arg3NH1	Glu97O	2.85

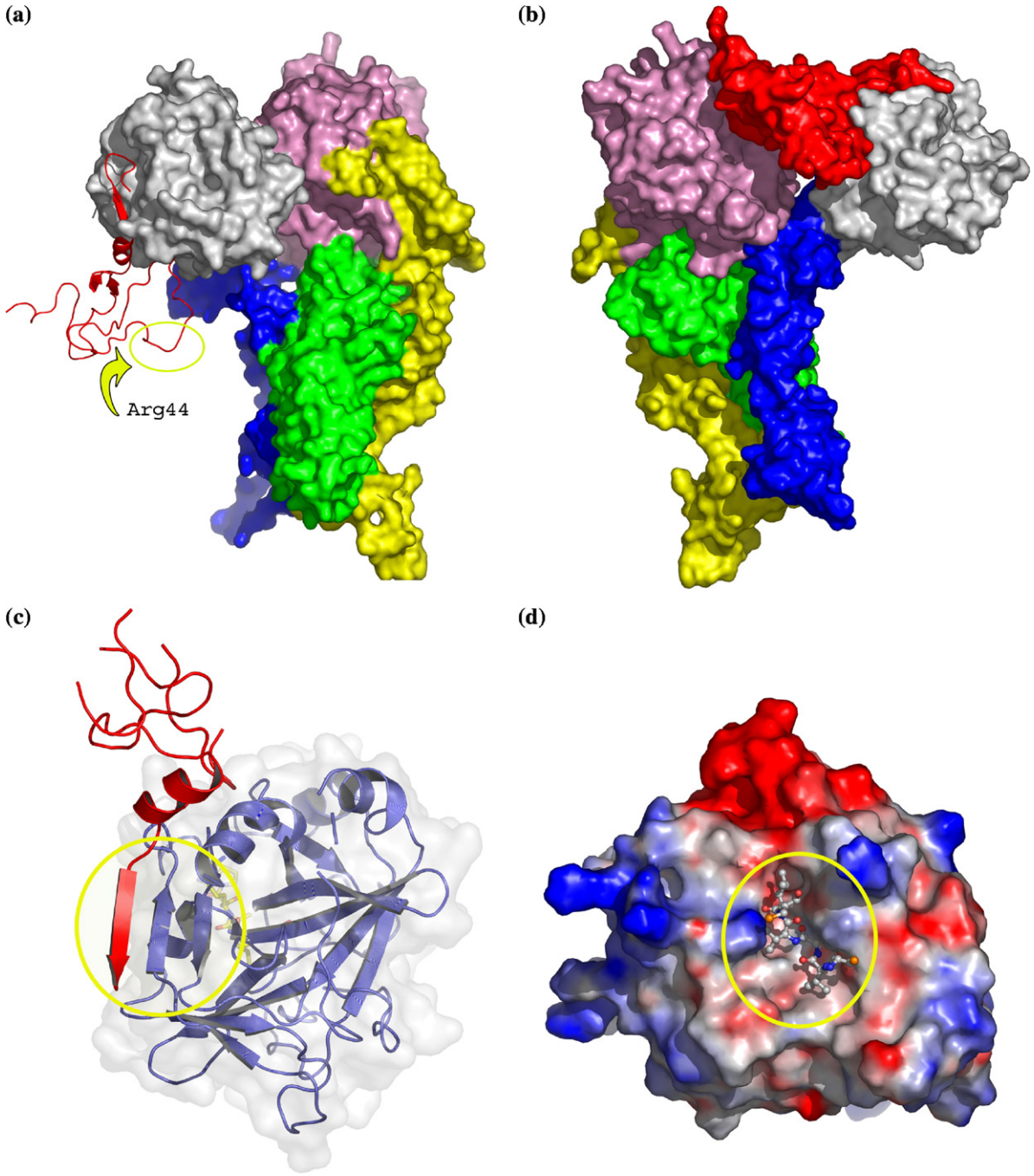

Figure 3. (a) Surface representation of the model of the complex TF (green), fVIIa (catalytic domain in pink and EGF1, EGF2 and Gla domains in yellow), fX (catalytic domain in gray and EGF1, EGF2 and Gla domains in blue). NAPc2 is in red (ribbon representation), yellow circle and arrow indicate the position of the insertion-loop containing the P1 (Arg44) residue. (b) Same as (a) but with the fXa re-positioned to permit the simultaneous binding of NAPc2 to the fXa exosite and the fVIIa active site. (c) Ribbon representation of the fXa-NAPc2 complex. The yellow circle indicates the antiparallel β-strand interactions between NAPc2 (red) and fXa (dark blue). (d) Surface charge of fVIIa with the modeled peptide fragment of the NAPc2 insertion-loop containing Arg44 in the active site cavity.

observed in the NMR structures and the C-terminal region of NAPc2.

Despite the high sequential (>54%) and structural homology between NAPc2 and NAP5 the mechanism of inhibition of fXa is different for NAP5 (active site inhibition, Figure 4(c)) and NAPc2 (Figure 4(a) and (c)).[7] Analogous to the reactive-site NAP5 P1 residue Arg40, NAPc2 contains an arginine at position 44 that likely interacts with the active site of fVIIa.

Interestingly, in the crystal structure of the binary complex of fXa/NAP5, a similar interaction is observed with relation to a symmetry-related fXa molecule, wherein the C terminus of NAP5 inter-

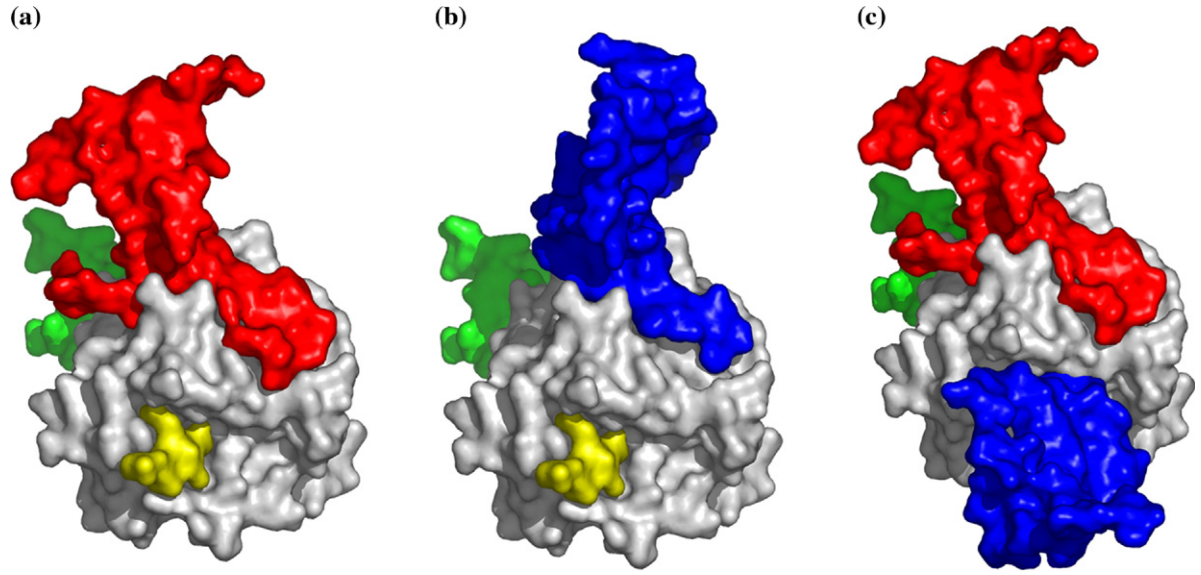

Figure 4. Active and exosite interactions: fXa (gray), EGF2 (green), selectide (yellow), NAPc2 (red) and NAP5 (blue). (a) The model of the fXa-NAPc2-selectide complex indicating the relative position of the exosite in relation to the active site. (b) The similar interaction of NAP5 with a symmetry-related fXa molecule at the exosite (J.R.S. and A.T., unpublished results). (c) Exosite binding of NAPc2 and active site binding of NAP5.

acts with this exosite (Figure 4(b)) (unpublished results).

Insights into the inhibition of the TF/fVIIa/fXa complex

The ternary complexes TF/fVII/fXa, TF/fVIIa/fX, and TF/fVIIa/fXa are of interest as targets for the inhibition of both the coagulation and cell-signaling pathways that are pivotal in cardiovascular disease and inflammation. In order to elucidate the mode of inhibition of TF/fVIIa by NAPc2 bound to fXa, the missing regions of NAPc2 were completed using the diffuse electron density and the NMR models as guides, since the important insertion-loop (31–49 loop) that contains the scissile bond Arg44–Val45 is disordered in the fXa-NAPc2-selectide complex. The interaction of NAPc2 with the catalytic site of fVIIa results in the insertion of the 31–49 loop that contains the cleavage site formed by Arg44. This loop region of the inhibitor was predicted to form the reactive sequence based on the sequence of analogous domains in similar small protein inhibitors of serine proteases[7] and compared with the structure of the NAP5-fXa complex (J.R.S. and A.T., unpublished results).

The proposed theoretical model of the TF/fVIIa/fXa complex built based on the available structures of the TF/fVIIa complex and fXa by protein–protein docking calculations and site-directed mutagenesis indicates that the fXa model adopts an extended conformation, similar to that of fVIIa in the TF/fVIIa complex, forming extensive interactions with TF and the protease domain of fVIIa. All four domains of fXa are involved in the interaction and the residues Glu51 and Asn57 in the EGF1 domain, Asp92 and Asp95 in the EGF2 domain and Asp185, Lys186, and Lys134 in the serine protease domain of fXa participate in the interaction with TF/fVIIa (PDB entry: 1NL8).[29]

Superpositioning the atomic coordinates of the NAPc2/fXa complex on the coordinates of the theoretical model of the TF/fVIIa/fXa complex indicates that the position of the NAPc2 insertion-loop containing the P1 (Arg44) residue is located more than 20 Å from the active-site pocket of fVIIa, thus being unable to simultaneously inhibit fVIIa and fX/Xa (Figure 3(a)). In order to obtain a more compatible model, the serine protease domain of fXa was re-positioned to permit the simultaneous interaction of NAPc2 with both the exosite of fXa and the active site of fVIIa (Figure 3(b)) without altering the interactions formed between the EGF and Gla domains of fXa with TF. In the absence of the crystal structure of the ternary complex fXa/fVIIa/TF that would precisely delineate the interface involved, the insertion-loop containing the P1 (Arg44) residue was modeled at the active site of fVIIa based on the crystal structure of the binary complex fXa-NAP5 (J.R.S. and A.T., unpublished results; Figure 3(d)). In this model, the side-chain of Arg44 occupies the S1 specificity site of fVIIa adopting an extended conformation and forming a N–O salt-bridge through its guanidium group and carboxylate oxygen atoms of Asp189. Val43, the P2 residue, is in close proximity to His57 and Lys60. Additionally, Leu42 is positioned optimally at the P3 position of the substrate forming hydrophobic contacts with Trp215 of fVIIa. Another valine residue (Val45) occupies the P1′ position followed by Cys46 at the P2′ position.

Bovine fXa *versus* human fXa

A weaker interaction (K_d = 260–500 nM) has been reported for the binding of NAPc2 with bovine fXa,

but the high affinity was restored to a recombinant chimeric bovine fX derivative containing 25 residues from the COOH terminus of the serine proteinase domain of human fX, suggesting that this region is responsible for species selectivity.[9] The lower affinity interaction between NAPc2 and bovine fXa is correlated with a more rapid elimination half-life of ~87 min in this species *versus* days in humans. Significant differences between the C terminus of bovine and human fXa are observed in the C-terminal region (244 to 251), which is structurally highly flexible in human fXa. This motif is ordered in only one structure of human fXa[10] (PDB entry: 1HCG) that is similar to bovine fXa. Upon NAPc2 binding to human fXa, the C-terminal region of fXa adopts a different conformation, by moving outwards as observed in the crystal structure (1HCG). Superpositioning the structures of bovine and human fXa (PDB entry: 1HGC) with the structure of human fXa bound to NAPc2 indicates the presence of several short contacts between the C-terminal regions (244–251) of bovine fXa and human fXa and the C-terminal extension of NAPc2. Sequence alignments of both bovine and human fXa indicate a high degree of sequence homology in the region 237 to 244, the exception being Ile241 in the bovine enzyme that is changed to Ser241 in the human enzyme. Ser241 does not participate in the binding of NAPc2 to human fXa, but the substitution of serine by isoleucine would prevent the approach and binding of NAPc2, resulting in steric clashes with Leu72, Met75 and Phe77. Another significant difference is observed in the 245–251 region of the C terminus; human fXa possesses predominantly positively charged residues (Gly-Leu-Pro-Lys-Ala-Lys), whereas this region in bovine fXa is mainly hydrophobic (Ala-Gly-Ala-Ala-Gly-Ser). Since this region does not participate in the binding of NAPc2 and is flexible, it likely does not play an important role in the binding of NAPc2 in either human or bovine fXa.

Functional implications and concluding remarks

The fVIIa/TF complex is an attractive target for the development of new anticoagulant drugs due to its strategic position in the blood coagulation cascade. Since NAPc2 binds to catalytically active, inhibited and a mutant of zymogen fX with similar affinities it represents a new class of fX/Xa and fVIIa/TF complex inhibitors with potential applications in the prevention and treatment of venous and arterial thrombosis and in the control of disseminated intravascular coagulopathies.

The crystal structure of the ternary fXa-NAPc2-selectide complex in conjunction with the biochemical results currently available; provide further insights in understanding its unique mechanism for fVIIa/TF inhibition. NMR and crystallographic results indicate that NAPc2 is extremely flexible even after binding to fXa, however, the C-terminal region becomes structured after binding to fXa and a large conformational change occurs resulting in the formation of an antiparallel β-sheet formed by residues 87–93 in the C-terminal region of fXa and residues 74–80 of NAPc2.

Despite the high specificity of fXa for arginine residues in the S1 specificity pocket, TyrD1 and not Arg3 occupies this position in the selectide inhibitor. TyrD1 does not directly interact with Asp189 but occludes the entrance of the S1 specificity pocket maintained by water-mediated interactions between the hydroxyl group of TyrD1 with the carbonyl oxygen of Ile227 and the carboxylate group of Asp189OD1.

These structural results and the delineation of the till now elusive exosite shed light on the direct inhibition of fXa and suggest modes for the indirect inhibition of VIIa.

Materials and Methods

Preparation and crystallization of the ternary complex

Human des-fXa[30] was purchased from Haematologic Technologies, Inc. Recombinant NAPc2[31] and the selectide inhibitor (TyrD-Ile-Arg-Leu-Prn; SEL2060) were provided by Corvas International, Inc and Selectide Corp., respectively. A molar ratio of 1.2:1.2:1 of NAPc2 and selectide to des-fXa was equilibrated overnight at 4 °C, dialyzed to remove excess ligands and concentrated to 10 mg/ml in 50 mM Tris-HCl, 20 mM NaCl buffer (pH 7.5). Single crystals of the ternary complex were obtained by the hanging-drop vapour-diffusion crystallization method where 1 μl of the complex was mixed with an equal volume of the reservoir solution containing 0.05 M potassium dihydrogen phosphate, 0.1 M sodium acetate (pH 5.6) and 16% (w/v) polyethylene glycol 8000.

Data collection, processing, structure determination and refinement

X-ray diffraction data were collected from cryo-protected crystals at 100 K at the Advanced Photon Source (IMCA-CAT beamline, Argonne National Laboratory) where the wavelength was set to 1.0 Å, a MAR-CCD detector was used to record the diffraction intensities and the data were reduced and scaled using the DENZO/SCALEPACK suite of programs.[32] The crystals belong to the orthorhombic space group $P2_12_12_1$ with cell dimensions $a=48.94$, $b=86.41$ and $c=145.89$ Å. The orientation and position of the catalytic and EGF2 domains of des-fXa were determined with the program AMoRe[33] using the coordinates of the same modules of native des-fXa[10] (PDB code 1HCG) stripped of solvent molecules. Examination of the $(2F_o–F_c)$ and $(F_o–F_c)$ difference electron density maps revealed density corresponding to segments of the NAPc2 molecule bound to the C terminus and β-strand (B5) of fXa and the selectide inhibitor bound at the active-site cleft. However, no electron density was present to account for the EGF1 domain as reported previously for both the native[10] and inhibited des-fXa structures.[12,13] The NAPc2 structure was determined by manual iterative interpretation of the electron density maps. The residues 1–5, 15–20 and 34–49 are highly disordered and were not included in the model during the refinement. In the final stages, the complete structure of NAPc2 was modeled based on the NMR structures using regions characterized

by diffuse density as a guide. Positional and restrained isotropic *B*-factor refinements were performed using REFMAC5,[34] all model building was carried out utilizing TURBO-FRODO[35] and PROCHECK[36] was utilized to evaluate the stereochemistry of the final structural model. Statistics of the intensity data processing and refinement are presented in Table 1.

Protein Data Bank accession code

The atomic coordinates and structure factors of human Gla-domainless factor Xa complexed with the anticoagulant protein NAPc2 from the hematophagous nematode *Ancylostoma caninum* and selectide inhibitor have been deposited with the RCSB Protein Data Bank, entry code 2H9E, Research Collaboration for Structural Bioinformatics, Rutgers University, New Brunswick, NJ†.

Acknowledgements

We are grateful to Dr G. Vlasuk for the NAPc2 samples used in this study and for critically reading the manuscript. This work was supported by grants from FAPESP (04/13082-3; 04/11258-0), CAPES/PROBRAL/DAAD (186/04), SMOLBNet (01/07537-2), CNPq (473097/2004-4; 501500/2005-7) and CAT/CEPID to R.K.A.; Michigan Economic Development Corp. to A.T. and J.H.G. and NIH grant HL43229 to A.T. M.T.M. is the recipient of a FAPESP (04/13054-3) fellowship.

References

1. Mann, K. G., Nesheim, M. E., Church, W. R., Haley, P. & Krishnaswamy, S. (1990). Surface-dependent reactions of the vitamin K-dependent enzyme complexes. *Blood*, **76**, 1–16.
2. Suttie, J. W. (1985). Vitamin K-dependent carboxylase. *Annu. Rev. Biochem.* **54**, 459–477.
3. McMullen, B. A., Fujikawa, K., Kisiel, W., Sasagawa, T., Howald, W. N., Kwa, E. Y. & Weinstein, B. (1983). Complete amino acid sequence of the light chain of human blood coagulation factor X: evidence for identification of residue 63 as beta-hydroxyaspartic acid. *Biochemistry*, **22**, 2875–2884.
4. Fernlund, P. & Stenflo, J. (1983). Beta-hydroxyaspartic acid in vitamin K-dependent proteins. *J. Biol. Chem.* **258**, 12509–12512.
5. Davie, E. W., Fujikawa, K. & Kisiel, W. (1991). The coagulation cascade: initiation, maintenance, and regulation. *Biochemistry*, **30**, 10363–10370.
6. Cappello, M., Vlasuk, G. P., Bergum, P. W., Huang, S. & Hotex, P. (1995). Ancylostoma caninum anticoagulant peptide: a hookworm-derived inhibitor of human coagulation factor Xa. *Proc. Natl Acad. Sci. USA*, **92**, 6152–6156.
7. Stanssens, P., Bergum, P. W., Gansemans, Y., Jespers, L., Laroche, Y., Huang, S. *et al.* (1996). Anticoagulant repertoire of the hookworm Ancylostoma caninum. *Proc. Natl Acad. Sci. USA*, **93**, 2149–2154.
8. Waxman, L., Smith, D. E., Arcuri, K. E. & Vlasuk, G. P. (1990). Tick anticoagulant peptide (TAP) is a novel inhibitor of blood coagulation factor Xa. *Science*, **248**, 586–593.
9. Buddai, S. K., Toulokhonova, L., Bergum, P. W., Vlasuk, P. & Krishnaswamy, S. (2002). Nematode anticoagulant protein c2 reveals a site on factor Xa that is important for macromolecular substrate binding to human prothrombinase. *J. Biol. Chem.* **277**, 26689–26698.
10. Padmanabhan, K., Pdmanabhan, K. P., Tulinsky, A., Park, C. H., Bode, W., Huber, R. *et al.* (1993). Structure of human des(1–45) factor Xa at 2.2 A resolution. *J. Mol. Biol.* **232**, 947–966.
11. Brandstetter, H., Kuhne, A., Bode, W., Huber, R., von der Saal, W., Wirthensohn, K. & Engh, R. A. (1996). X-ray structure of active site-inhibited clotting factor Xa. Implications for drug design and substrate recognition. *J. Biol. Chem.* **271**, 29988–29992.
12. Wei, A., Alexander, R. S., Duke, J., Ross, H., Rosenfeld, S. A. & Chang, C. H. (1998). Unexpected binding mode of tick anticoagulant peptide complexed to bovine factor Xa. *J. Mol. Biol.* **283**, 147–154.
13. Kamata, K., Kawamoto, H., Honma, T., Iwama, T. & Kim, S.-H. (1998). Structural basis for chemical inhibition of human blood coagulation factor Xa. *Proc. Natl Acad. Sci. USA*, **95**, 6630–6635.
14. Orthner, C. L. & Kosow, D. P. (1978). The effect of metal ions on the amidolytic acitivity of human factor Xa (activated Stuart-Prower factor). *Arch. Biochem. Biophys.* **185**, 400–406.
15. Orthner, C. L. & Kosow, D. P. (1980). Evidence that human alpha-thrombin is a monovalent cation-activated enzyme. *Arch. Biochem. Biophys.* **202**, 63–75.
16. Steiner, S. A., Amphlett, G. N. & Castellino, F. J. (1980). Stimulation of the amidase and esterase activity of activated bovine plasma protein C by monovalent cations. *Biochem. Biophys. Res. Commun.* **94**, 340–347.
17. Zhang, E. & Tulinsky, A. (1997). The molecular environment of the Na^+ binding site of thrombin. *Biophys. Chem.* **63**, 185–200.
18. Strickland, D. K. & Castellino, F. J. (1980). The binding of calcium to bovine factor VII. *Arch. Biochem. Biophys.* **190**, 687–692.
19. Bajaj, S. P., Sabharwal, A. K., Gorka, J. & Birktoft, J. J. (1992). Antibody-probed conformational transitions in the protease domain of human factor IX upon calcium binding and zymogen activation: putative high-affinity Ca(2+)-binding site in the protease domain. *Proc. Natl Acad. Sci. USA*, **89**, 152–156.
20. Bode, W. & Schwager, P. (1975). The refined crystal structure of bovine beta-trypsin at 1.8 A resolution. II. Crystallographic refinement, calcium binding site, benzamidine binding site and active site at pH 7.0. *J. Mol. Biol.* **98**, 693–717.
21. Dougherty, D. A. & Stauffer, D. A. (1990). Acetylcholine binding by a synthetic receptor: implications for biological recognition. *Science*, **250**, 1558–1560.
22. Stauffer, D. A., Barrans, R. E. & Dougherty, D. A. (1990). Concerning the thermodynamics of molecular recognition in aqueous and organic media. Evidence for significant heat capacity effects. *J. Org. Chem.* **55**, 2762–2767.
23. Schwabacher, A. W., Zhang, S. & Davy, W. (1993). Directionality of the cation-π effect: a charge-mediated size selectivity in binding. *J. Am. Chem. Soc.* **115**, 6995–6996.
24. Lim, Z. & Johnson, M. E. (1995). Proposed cation-π mediated binding by factor Xa: a novel enzymatic

† http://www.rcsb.org/

mechanism for molecular recognition. *FEBS Letters*, **370**, 1–5.
25. St. Charles, R., Padmananbhan, K., Arni, R. K., Padmanabhan, K. P. & Tulinsky, A. (2000). Structure of tick anticoagulant peptide at 1.6 Å resolution complexed with bovine pancreatic trypsin inhibitor. *Protein Sci.* **9**, 256–272.
26. Mochalkin, I. & Tulinsky, A. (1999). Structures of thrombin retro-inhibited with SEL2711 and SEL2770 as they relate to factor Xa binding. *Acta Crystallog. sect. D*, **55**, 785–793.
27. Duggan, B. M., Dyson, H. J. & Wright, P. E. (1999). Inherent flexibility in a potent inhibitor of blood coagulation, recombinant nematode anticoagulant protein c2. *Eur. J. Biochem.* **265**, 539–548.
28. Harley, B. S. & Shotton, D. M. (1971). Pancreatic elastase. In *The Enzymes* (Boyer, P. D., ed), 1st edit., pp. 323–373. Academic Press, New York.
29. Norledge, B. V., Petrovan, R. J., Ruf, W. & Olson, A. J. (2003). The tissue factor/factor VIIa/factor Xa complex: a model built by docking and site-directed mutagenesis. *Proteins: Struct. Funct. Genet.* **53**, 640–648.
30. Morita, T. & Jackson, C. M. (1986). Preparation and properties of derivatives of bovine factor X and factor Xa from which the gamma-carboxyglutamic acid containing domain has been removed. *J. Biol. Chem.* **261**, 4015–4023.
31. Laroche, Y., Storme, V., De Meutter, I., Messens, J. & Lauwereys, M. (1994). High-level secretion and very efficient isotopic labeling of tick anticoagulant peptide (TAP) expressed in the methylotrophic yeast, *Pichia pastoris*. *BioTechnology*, **12**, 1119–1124.
32. Otwinoski, Z. & Minor, W. (1997). Processing of X-ray diffraction data collection in oscillation mode. *Methods Enzymol.* **276**, 307–326.
33. Navaza, J. (1993). AMoRe: an automated package for molecular replacement. *Acta Crystallog. sect. D*, **49**, 588–591.
34. Murshudov, G. N., Vagin, A. A. & Dodson, E. J. (1997). Refinement of macromolecular structures by the maximum-likelihood method. *Acta Crystallog. sect. D*, **53**, 240–255.
35. Roussel, A. & Cambillau, C. (1989). Turbo-Frodo. In *Silicon Graphics Geometry Partner Directory* (Silicon Graphics, ed), pp. 77. Mountain View, CA.
36. Laskowski, R. A., MacArthur, M. W., Moss, D. S. & Thorton, J. M. (1993). PROCHECK: a program to check the stereochemical quality of protein structures. *J. Appl. Crystallog.* **26**, 283–291.

Edited by R. Huber

(Received 7 August 2006; received in revised form 4 November 2006; accepted 9 November 2006)
Available online 14 November 2006